17

Improving Machining Accuracy Using Smart Materials

Maki K. Rashid

1. Introduction

Both economical and ecological factors might encourage conventional machines to continue in service by healing tool vibration problems. Higher productivity in automated manufacturing system brought to the attention the importance of machine tool error elimination. Various factors might affect the machining process (Merritt, 1965), some of them are non-measurable, and others might change in real-time. However, the wider use and availability of suitable and economical microcontrollers encouraged the use of intelligent control scheme to overcome such time dependent problem. Large magnitude of excitation forces with a tiny relative motion between cutting tool and working piece promote the use of smart material actuators that interfaced with microcontrollers to counteract such motion errors (Dold, 1996). Rigid fixture is a requirement to minimize displacements of cutting tools from its nominal position during machining. However, the reconfigurable manufacturing era encourage the use of small fixtures with lower mass (Gopalakrishnan, et al., 2002) and (Moo n& Kota, 2002).

Previous dynamic modeling of a smart toolpost (Frankpitt, 1995) is based on linear piezo-ceramic actuator. The system is either modeled as lumped single rigid mass incorporating tool carrier (holder), tool bit, and piezo-actuator. Or by using an effective mass, stiffness, and, damping coefficients for the most dominant mode of vibration. The fundamentals of this model are incorporated to design an adaptive controller using the measured current, and, voltage applied to the actuator as a control signals. Based on identical principles (Eshete, 1996) and (Zhang et al., 1995) a mathematical model is derived for smart tool post using PMN ceramic material. A control system, and real time microprocessor implementation was examined in (Dold, 1996]. Sensitivity analysis for the toolpost design modifications and interfacing parameters on tool dynamic response require further elaboration. No conclusions are drawn related to better design and selection of actuator, tool holder and tool bit stiffness ratios. In

Source: Manufacturing the Future, Concepts - Technologies - Visions , ISBN 3-86611-198-3, pp. 908, ARS/plV, Germany, July 2006, Edited by: Kordic, V.; Lazinica, A. & Merdan, M.

case of a future geometrical change, the validity of the lumped masses in system modeling is questionable. Nature and type of signals that control smart material actuator and how can affect toolpost dynamic response suffer from scarcity of information. Recently a systematic engineering approach is used to investigate an optimum fixture–workpiece contacts property (Satyanarayana & Melkote, 2004), machining fixtures dimension (Hurtado & Melkote, 2001) and structural stiffness in toolpost dynamic (Rashid, 2004) by using the finite element approach.

Present analysis investigates the capability of smart material in tool error elimination using finite element modeling. This incorporates structural stiffness evaluations for toolpost actuator, tool holder, holder fixture, and tool bit. Radial tool movement relative to the workpiece is regarded as a main source for cutting tool error. Considerations are given for evaluating lumped mass modeling, effectiveness of dynamic absorber in case of PWM voltage activation and effect of toolpost stiffness ratios on error elimination. Awareness is given for the model to be capable of handling large variations in design parameters for future toolpost development in the case of limited space and weight requirements. Other issues are related to the effectiveness of dynamic absorber presence, switching rate and voltage modifications to minimize tool error.

2. Toolpost FEM Model

In this work the Lead Zirconate Titanate (PZT), is the intelligent material for the investigated smart toolpost actuator. This encouraged by the well-developed theoretical analysis of this material and its common use. Two models are applied for obtaining the toolpost results. The first is shown in Fig. 1 (a) represented by actuator, tool carrier (holder), diaphragm support and tool bit as a spring buffer between tool carrier and the axially actuated cutting force at tool tip (radial to the work piece). The second model in Fig. 1 (b) is added to it the dynamic absorber as a disk supported by a diaphragm. In this work 8-node isoparametric solid element is used for domain discretization. The FEM model is tested in terms of mesh refinement, and, the results compared to a similar verified analytical work. Maximum difference between calculated values throughout verifications is within 8%.

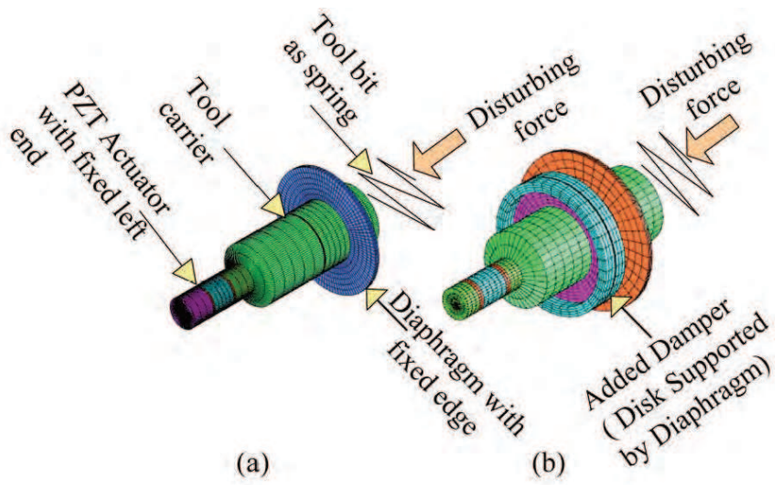

Figure 1. Toolpost Models

Conventional stacked PZT actuator incorporates polarized ferroelectric ceramic in the direction of actuation, adhesive, supporting structure, and electrodes wired electrically as shown in Fig. 2.

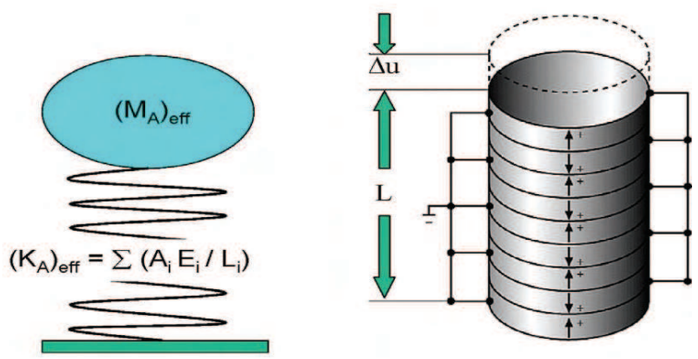

Figure 3. PZT Stacked Actuator

Modeling of active materials and toolpost are based on the general constitutive equations of linear piezoelectricity and the equations of mechanical and electrical balance (Piefort, V. 2001). The equations are thus expressed as

$$\begin{aligned} \{T\} &= [c^E]\{S\} - [e]^T\{E\} \\ \{D\} &= [e]\{S\} + [\varepsilon^S]\{E\} \end{aligned} \tag{1}$$

The momentum balance equation is

$$\rho\{\ddot{u}\} = \nabla.\{T\} \tag{2}$$

Moreover, the electric balance equation is

$$\nabla.\{D\} = 0 \tag{3}$$

Known $\{S\} = \nabla^S.\{u\}, \qquad \{E\} = -\nabla\phi$

Where $\{T\}$ represents the stress vector, $\{S\}$, the strain vector, $\{E\}$, the electric field, $\{D\}$, the electric displacement, $[c^E]$, the elastic coefficients at constant $\{E\}$, $[\varepsilon^S]$, the dielectric coefficients at constant $\{S\}$, and $[e]$, the piezoelectric coupling coefficients. $\{u\}$ is the mechanical displacement vector and $\{\ddot{u}\} = \partial^2\{u\}/\partial t^2$ is the acceleration. ϕ is the electric potential (voltage). The boundary conditions are expressed in Fig. 1, where zero displacements are assigned to actuator left end and, fixed outer edge for supporting diaphragm. Problem description is finalized by assigning voltage to actuator electrodes and applying force at tool tip.

The unknowns are the displacements vector u_i and the electric potential values ϕ_i at node i. The displacement and voltage fields at arbitrary locations within elements are determined by a linear combination of polynomial interpolation or shape functions N_u and N_ϕ respectively. The nodal values of these fields are used as coefficients. The displacement field $\{u\}$ and the electric potential ϕ over an element are related to the corresponding node values $\{u_i\}$ and $\{\phi_i\}$ by the mean of the shape functions$[N_u]$, and $[N_\phi]$

$$\begin{aligned} \{u\} &= [N_u]\{u_i\} \\ \phi &= [N_\phi]\{\phi_i\} \end{aligned} \tag{4}$$

The dynamic equations of a piezoelectric continuum derived from the Hamilton principle, in which the Lagrangian and the virtual work are properly adapted to include the electrical contributions as well as the mechanical ones (Piefort, 2001 et al., 1990). Taking into account the constitutive Eqs. (1) and substituting the LaGrangian and virtual work into Hamilton's principle to yields variational equation that satisfy any arbitrary deviation of the displacements $\{u_i\}$ and electrical potentials $\{\phi_i\}$ compatible with the essential boundary conditions, and then incorporate Eq. (4) to obtain

$$\begin{aligned} [m_{uu}]\{\ddot{u}_i\} + [c_{uu}]\{\dot{u}_i\} + [k_{uu}]\{u_i\} + [k_{u\phi}]\{\phi_i\} &= \{f_i\} \\ [k_{u\phi}]^T\{u_i\} + [k_{\phi\phi}]\{\phi_i\} &= \{q_i\} \end{aligned} \tag{5}$$

$[m_{uu}]$, $[k_{uu}]$ and, $[c_{uu}]$ are the mechanical mass, stiffness and damping matrices, respectively. $[k_{u\phi}]$ is the piezoelectric coupling matrix. $[k_{\phi\phi}]$ is the dielectric stiffness matrix. $\{f_i\}$ and $\{q_i\}$ are the nodal mechanical force and electric charge vectors, respectively. $\{u_i\}$ and, $\{\phi_i\}$ are the nodal displacement and potential vectors, respectively. For the sake of brevity, (Zienkiewicz & Taylor, 2000) discuss the scheme by which the elemental contributions are assembled to form the global system matrices.

3. Lumped Versus FEM Modeling

Lumped mass modeling for PZT actuator and tool carrier produce simple closed form solutions that are of interest to the designer and modeler (Frankpitt, 1995 and, Piefort, 2001). However, model validity of such representation for different design applications deserves more attention. In some applications, smart materials are used simultaneously in sensing and actuation. Displacement sensing at different locations is dependent on system dynamic, design geometry and system rigidity. Controller effectiveness relies on a valid dynamic system representation and the limits of legitimacy of such model.

A comparative result for a deviation in natural frequency of lumped mass versus continuous system is discussed for a single actuator as a first step toward an integrated tool post.

3.1 Comparative Results for Actuator Modeling

Before solving the time-dependent equation of motion for the smart toolpost, the mode shapes and the resonant frequencies of undamped system are obtained by using Eigenvalue analysis. The Eigenvalue problem is carried using a reduced matrix system obtained by matrix condensation of structural and potential degrees of freedom. Free vibration implies

$$\{[K^*] - \omega^2[m_{uu}]\}\{U_i\} \tag{6}$$

Where ω is the natural frequency, the new stiffness matrix $[K^*]$ indicates that structure is electromechanically stiffened. The modal analysis is based on the orthogonality of natural modes and expansion theorem (Zienkiewicz, and Taylor, 2000 a & b). Usually the actuator is composed off several PZT layers, electrodes, adhesive, and supporting structure as shown in Fig. 2. The effective stiffness of the actuator (***STIFA***) is the stiffness summation of all individual layers neglecting all piezoelectric effects.

$$(K_A)_{eff} = STIFA = \sum(\frac{A_i E_i}{L_i}) \tag{7}$$

For comparison the effective actuator mass assumed to be 20 or 30% of the layers masses as indicated in Fig. 3.

$$(M_A)_{eff} = (0.2 \quad or \quad 0.3)\sum(A_i \rho_i L_i) \tag{8}$$

Then

$$\omega_{Lumped} = \sqrt{\frac{(K_A)_{eff}}{(M_A)_{eff}}} \tag{9}$$

The FEM solution of the first natural frequency for short circuit and open circuit actuator are compared to the lumped mass frequency as obtained from Eq. (9) and the ratio is plotted in Fig. 3.

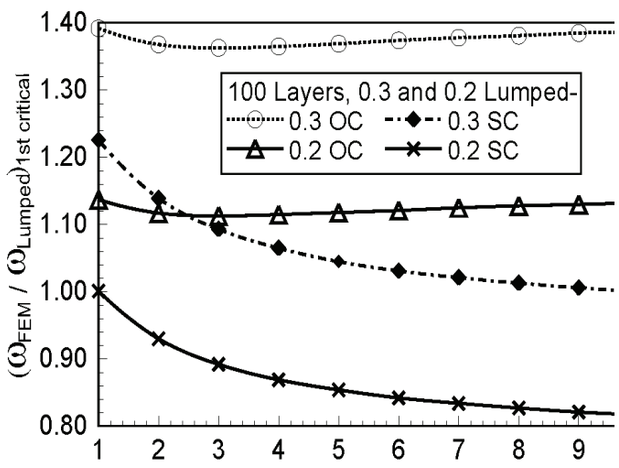

Figure 3. First critical frequency ratio /FEM/Lumped) versus layers thickness ratios for short circuit (SC) and open circuit (OC).

PZT8 properties from (Berlincourt, & Krueger, 2000) are used in FEM calculations. Plotted results in Fig. 3 are not incorporating stiffness variation resulted from actuator fabrication. Short circuit actuator shows a decrease in natural frequency, which indicates actuator stiffness reduction. Actuator short and open circuit conditions maps the two stiffness extremes and such data provide designers quick tool for estimating natural frequencies in early stages of design.

3.2 Comparative Results for Toolpost Model Incorporating Dynamic Absorber

In lumped modeling shown in Fig. 4 the tool carrier is considered as a rigid mass added to it one third of the PZT actuator mass and assigned (M_T). The dynamic absorber is the second mass (M_d) of the two-degree of freedom system and compared to the FEM solution to investigate lumped model validity of such system. A close form solution is obtained for the two-degree of freedom system incorporating the piezoelectric coupling effects (Frankpitt, 1995, and, Abboud, Wojcik, Vaughan, Mould, Powell, & Nikodym, 1998). Nevertheless, there solution does not answer the significant deviation between FEM and

lumped mass solutions in the case of no pizo effects. The supporting diaphragm stiffness (K_D) is calculated as a plate with central hole fixed at both inner and outer edges (Roark, and Young, 1975) then, added to actuator stiffness to form a cushion for tool carrier.

The actuator stiffness (K_A) is calculated as in Fig. 2. Then the dynamic absorber diaphragm stiffness for dynamic absorber (K_d) is considered as a plate with central hole fixed at both inner and outer edges

From Fig. 4 the equations of lumped mass and stiffness matrices for a two-degree of freedom system is:

$$[M]=\begin{bmatrix} M_T & 0 \\ 0 & M_d \end{bmatrix} \qquad (10)$$

$$[K]=\begin{bmatrix} K_A+K_D+K_d & -K_d \\ -K_d & K_d \end{bmatrix}$$

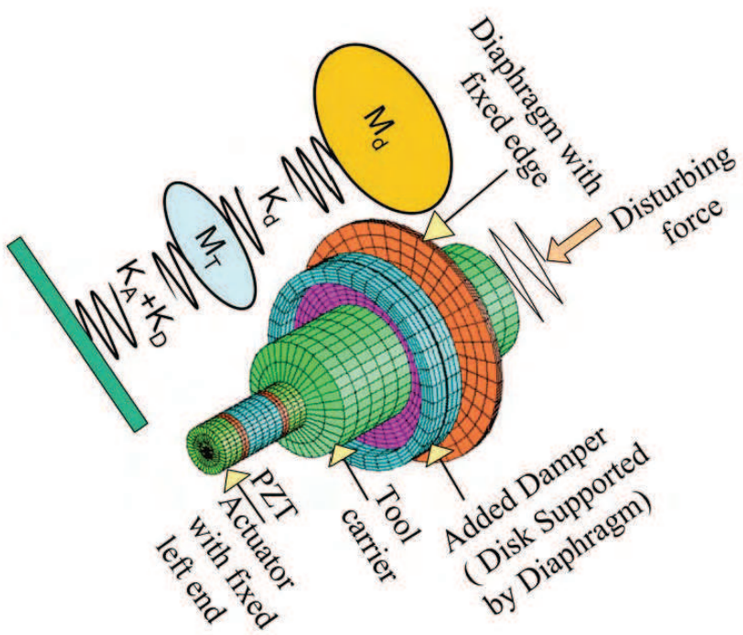

Figure 4. Tool post with dynamic absorber

Then the dynamic equation of motion and its characteristic equations for undamped free vibration can be derived as

$$\begin{aligned} &[M]\{\ddot{u}\}+[K]\{u\}=\{0\} \\ &-\omega_i^2[M]+[K]=0 \end{aligned} \tag{11}$$

Two natural frequencies are calculated from Eq. (11). Then lumped model frequencies (ω_{Lumped}) compared with the first three natural frequencies of the FEM model (ω_{FEM}) taking into consideration the mode shape and the Eigenvalue results. Three frequency ratios are compared namely $(\omega_{FEM})_{1st}/(\omega_{Lumped})_{1st}$ for 1st critical, $(\omega_{FEM})_{2nd}/(\omega_{Lumped})_{2nd}$ for 2nd critical, and $(\omega_{FEM})_{3rd}/(\omega_{Lumped})_{2nd}$ for 3rd critical.

Figure 5 show such variation of frequency ratios on log-log plot against the ratio of diaphragm support stiffness to actuator stiffness for a unit ratio between tool carriers to actuator stiffness (K_T/K_A). In general, the FEM model predicts lower natural frequencies for the toolpost and this deviation increases with the increase in the ratio of diaphragm support to actuator stiffness (K_D/K_A).

Increasing the ratio of tool carrier to actuator stiffness (K_T/K_A) ten times as in Fig. 5 yields a closer FEM solution to the lumped model at low diaphragm support to actuator stiffness ratio as shown in Fig. 6. However, the deviation again increases with the increase in diaphragm support to actuator stiffness ratio (K_D/K_A).

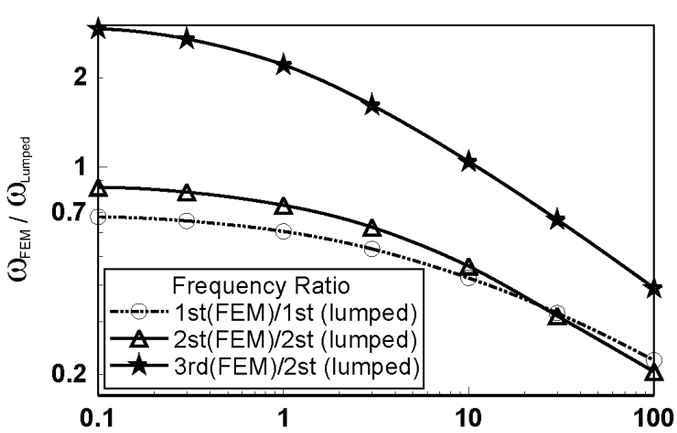

Figure 5. Frequency ratio of REM to lumped masses against diaphragm support to actuator stiffness (K_T/K_A=1.0, open circuit)

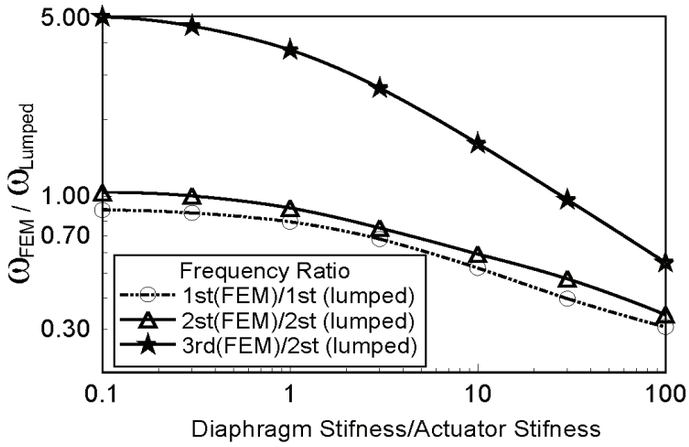

Figure 6. Frequency ratio of FEM to lumped masses against diaphragm support to actuator stiffness ratio (K_T/K_A = 10.0, open circuit)

Although the validity of lumped mass modeling can be defined in, a specific region but the broad requirement of design applications would limit the use of such narrow domain. As noticed, the critical frequencies are quite dependent on stiffness ratio and the FEM third critical can be the same as 2nd critical frequency of lumped mass modeling at high diaphragm stiffness ratio.

4. Results of Estimated Static Force Availability for Error Elimination

Elimination of error in tool positioning under static condition relies on PZT actuator capability in resisting axial tool force within the range of motion. To have initial guessing for the generated force a displacement curve is developed for the investigated PZT toolpost under static condition. Figure 7 shows such force-displacement characteristics at different levels of voltage intensity and for specified values of tool tip to actuator stiffness ratio (TIP-Ratio), diaphragm to actuator stiffness ratio (D-Ratio), and, tool carrier to actuator stiffness ratio (T-Ratio).

Calculations conducted in this work proved the importance of increasing tool tip to actuator stiffness, tool carrier to actuator stiffness and, reducing diaphragm to actuator stiffness ratios for a better utilization of actuator operating range. Figuring out an appropriate actuator for specific application is by relating the cutting force value to the information given in Fig. 7. However, such

information does not predict the required dynamic actuator voltage during service. Smart material data, toolpost dimensions and, actuator layers thicknesses are given in Table 1 for both static and transient force-displacements calculations.

Item	Value	Unit
Cylindrical PZT-8 Stack		
PZT Thickness	0.09e-	m
Electrode Thickness	0.03e-	m
Structural support	0.03e-	m
Adhesive Thickness	10.0e-	m
Number of layers	500	
Effective Radius	5.0e-3	m
Steel Cylindrical Tool Carrier (holder)		
Radius	10.0e-3	m
Length	65.35e-	m
Steel Tool Bit Effective Length		
Assumed Effective	20.0e-3	m
Steel Diaphragm		
Thickness	0.5e-3	m
Outside Radius	20.0e-3	m

Table 1 Toolpost dimension

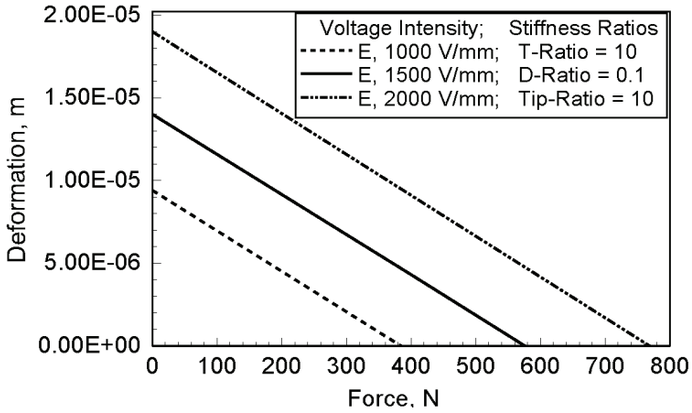

Figure 7. Tool load versus deformation for different PZT voltage intensity and fixed structural stiffnesses

5. Toolpost Time Response Due to Combined Effect of Voltage and Force Activation:

Evaluation of switching effects and system damping on toolpost response during error elimination are quantified by solving Eq. (5) in time domain for the system shown in Fig. 1. The PZT stack pattern is given in Table 1 that incorporates PZT layers, supporting structure, and electrodes for alternating poling direction. A thin layer of glue bonds wafers to one another. Because of this arrangement, the mechanical properties act in series. To reduce computational time the PZT stack is treated as a monolithic layer and precautions are taken accordingly for electric field intensity and other factors for multi-layer.

5.1 Voltage Switching Methodology

Deviation in position between tool tip and workpiece can be minimized by appropriate voltage activation to the PZT actuator. The easy way of activating smart material for vibration suppression is by using Pulse Width Modulation (PWM). It is a common technique available with the microcontroller units (MCU) to govern the time average of power input to actuators. Our main concern is the time dependent response accompanying the tool error suppression in using the PWM for smart material actuator. Voltage activation for smart material might either based on a piezo stack with force sensing layer or using an appropriate type of displacement sensor to detect tool carrier motion. In both methods sensing location should reflect cutting tool position error correctly. Switching circuits (Luan, and Lee, 1998) are not of our concern; however, the required voltage level and the resulted motion are among the targeted results in this work.

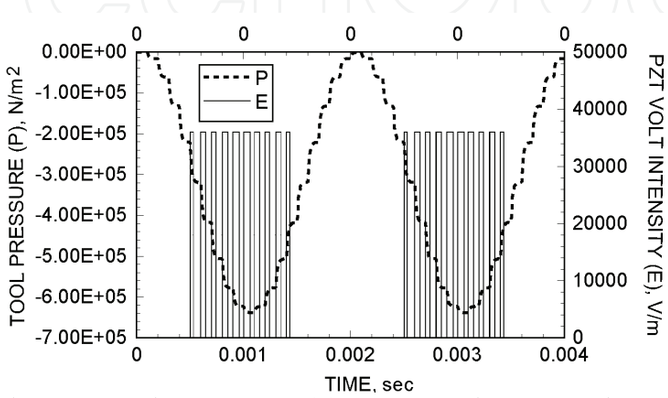

Figure 8. Tool carrier compressive presssure (P) accompanying PZT voltage activation intensity (E) plotted on a common time axis.

Figure 8 shows two cycles of voltage activation for the PZT actuator using PWM to oppose the compressive time dependent cutting force. The waveform of the compressive cutting force is used as a reference for the PWM voltage with a chance to incorporate the time delay. All present work results are assuming harmonic force actuation.

5.2 Solution Scheme for the Toolpost Time Response

The classical Newmark algorithm (Zienkiewicz, and Taylor, 2000b) solves the system of equations for such a nonlinear problem. Time step-by-step integration is used for solving Eq. (5) for the system shown in Fig. 1. This scheme assumes the system-damping matrix as linear combination of stiffness and mass matrices (Rayleigh damping) (Bathe, 1982):

$$[c_{uu}] = \alpha[m_{uu}] + \beta[k_{uu}] \tag{12}$$

Both α and β are constants to be determined from two proposed modal damping ratios (ξ_i) (1% and 5%) for first and second natural frequencies respectively which are obtained from the FEM model and the equation of modal damping as given in (Bathe, K.J. 1982).

5.3 Results for the Tool Time Transient Response

Synchronization of voltage activation with tool radial force can be reached either through a sensing layer in actuator stack or by using a displacement sensor for detecting tool carrier movements. The effective use of any of these techniques requires a profound investigation for toolpost dynamic behavior as related to its structural stiffness properties.

Tool dynamic and structural design for a reconfigurable machine tool (Gopalakrishnan, Fedewa, Mehrabi, Kota, & Orlandea, 2002, and, Moon & Kota, 2002] elevated new design challenges. Among them are methods for reducing tool holder size or developing a special tactics in using smart actuators for reaching targeted precision.

Tool cutting force predictions in dynamic calculations involve some difficulties due to the number of involved variables and the dynamic nature of the problem. In general approximate static force relation (Frankpitt, 1995) in terms of

depth of cut d (mm), cutting speed V (mm/s), feed f (mm/rev), and, coefficients describing nonlinear relationships ($\kappa, \lambda, and, \gamma$) can be used as first guess to express the general trends,

$$F_r(N) = K_r d^{\lambda} V^{\gamma} f^{\kappa}(t); \quad Where \quad K_r \text{ is a general constant.} \tag{13}$$

$F_r = K_r d^{\lambda} V^{\gamma} f^{\kappa}(t)$ K_r a general constant

The factors K_r, λ, γ and, κ are to be calibrated for each tool-workpiece. These constants are assigned to a specific material combinations, process types, tool-wear condition, workpiece hardness, tool geometry, and speed. Fluctuation of the cutting force is inherent and associated with cutting tool motion. Such randomness can vary with different cutting processes and material combinations.
For present results, toolpost dimension and, material are given in Table 1. Previous work (Rashid, M. K. 2004) indicated the use of few PWM, cycles per force period produced unfavorable switching dynamic excitation. Twenty PWM cycles for each force period produce good results more than forty has a little effect. In all calculations a value of ten is assigned to tool bit to actuator stiffness ratio (TIP-Ratio) and tool carrier to actuator stiffness ratio (T-Ratio). On the contrary, the diaphragm to actuator stiffness ratio (D-Ratio) assigned a low value of one tenth. The importances of such ratios are related to the force availability for error elimination and accurate displacement detection.
Figure 5 shows a tiny difference between resonant frequencies obtained from both FEM and lumped model solutions in case of existence of low diaphragm to actuator stiffness (D-Ratio) and high tool bit to actuator stiffness (TIP-Ratio) ratios. Under such conditions incorporating a classical dynamic absorber to a toolpost excited by harmonic inputs should attenuate vibration error. Our main concern is the effectiveness of such dynamic absorber for activated actuator by a PWM voltage instead of a continuous harmonic input voltage as the case in this work.
From classical dynamic absorber theory and for optimum damping, the applied force frequency must be tuned to absorber natural frequency. Also a mass ratio of 0.25 must be secured between dynamic absorber and tool carrier. Then the natural frequency ratio of absorber to tool carrier based on classical dynamic absorber under pure harmonic inputs and optimum-damping condition is obtained from Eq. (14). This natural frequency ratio is enforced to the FEM model by adjusting damper diaphragm stiffness in Fig. 4. Damper effec-

tiveness on error elimination is then compared to other toolpost design parameters under the condition of PWM voltage activation as shown in Figs. 9-13. Graph legends terminology of Figs. 9-13 are given in table 2.

$$\text{Natural frequency ratio of absorber to tool carrier} = \frac{1}{1+(M_d / M_T)} \tag{14}$$

No-A	No dynamic absorber
Y-A	Yes absorber is incorporated
Low-D	Low Damping
Hi-D	High Damping (10 x Low-D)
M-Sw	Modified mean voltage during Switching
Un-Sw	Un-modified mean voltage during Switching
No-volt	No voltage applied to actuator
Y-volt	Yes voltage applied to actuator

Table 2.

Figure 9 shows a significant error reduction can be attained by modifying the mean voltage of the PWM during the force actuation period. A single scheme is used for conducting voltage modification based on harmonic sine wave of the tool actuation force and described by the following set of equations:

If $|\sin \omega t| < 0.2$ then multiply present mean voltage by four,
If $|\sin \omega t| > 0.2$ and $\sin \omega t < 0.6$ do not change the mean voltage,
If $|\sin \omega t| > 0.6$ then multiply present mean voltage by (0.65).

Applying smart material actuator with unmodified mean voltage might deteriorate the error elimination process as shown in Figs. 9-13. Utilizing smart material for tool error elimination require assurance for both force sensing direction and proper voltage modification to reach the targeted beneficial results. Dynamic absorber effectiveness in error elimination is frequency dependent. Absorber presence in Figs. 9, 11 and 13 aggravated the error elimination improvement made by voltage modification. In all of these results, the dynamic

absorber natural frequency is tuned according to Eq. (14). Figures 9 and 11 are plotted for 2-cycles to improve comparison among error results. In Fig. 10, a small improvement is resulted due to the dynamic absorber presence but it is not a solid case to measure on. Figure 13 demonstrate a counteracting effect for the dynamic absorber even with existence of the applied modified voltage to the smart material actuator. The use of high damping (Hi-D) with ten folds the low damping (Low-D) does not have same effectiveness of using smart material actuator with properly modified mean voltage during the PWM. Conducted calculations demonstrated no significant effects for the time delay between applied voltage and activation force if the delay controlled to be within 10% of the force period.

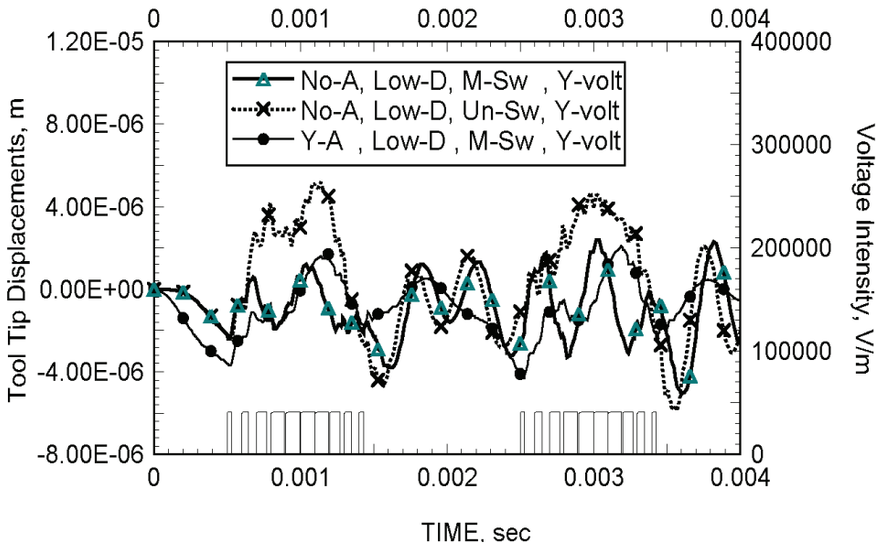

Figure 9. PZT Voltage Intensity and Tool tip displacements Versus time at 500 Hz

The estimated radial cutting force value from Eq. (13) and the static force-displacement relationship shown in Fig. 7 are important in initial guessing for the required applied voltage. But the final magnitude of dynamic applied voltage is deduced from the associated error resulted from the modification methodology for the mean voltage during PWM.

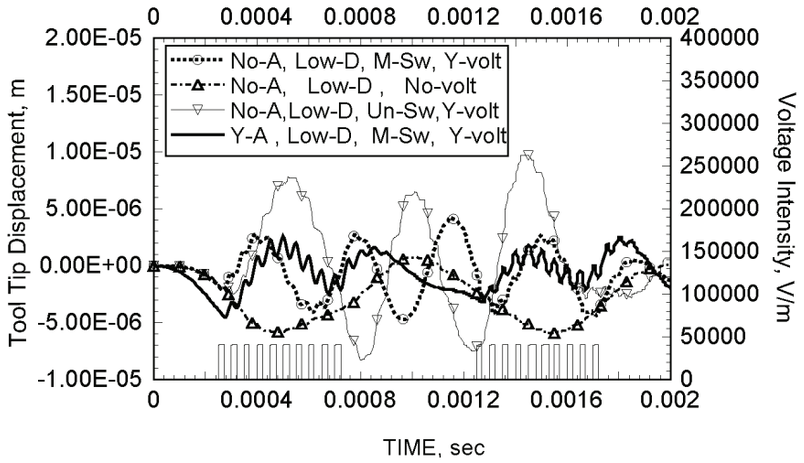

Figure 10. PZT Voltage Intensity and Tool tip displacements Versus time at 1000 Hz

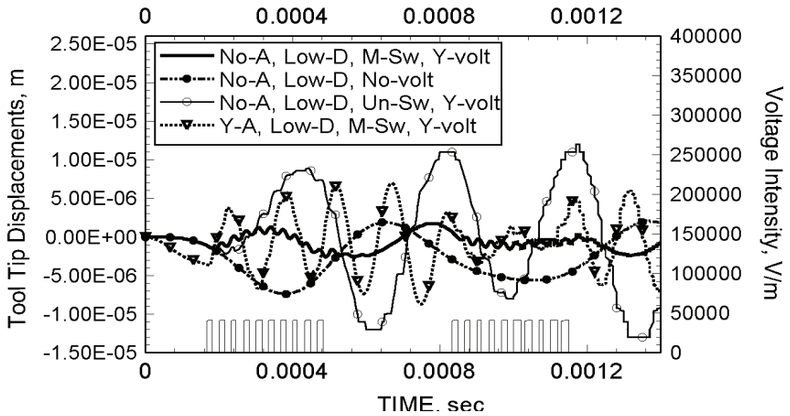

Figure 11. PZT Voltage Intensity and Tool tip displacements Versus time at 1500 Hz

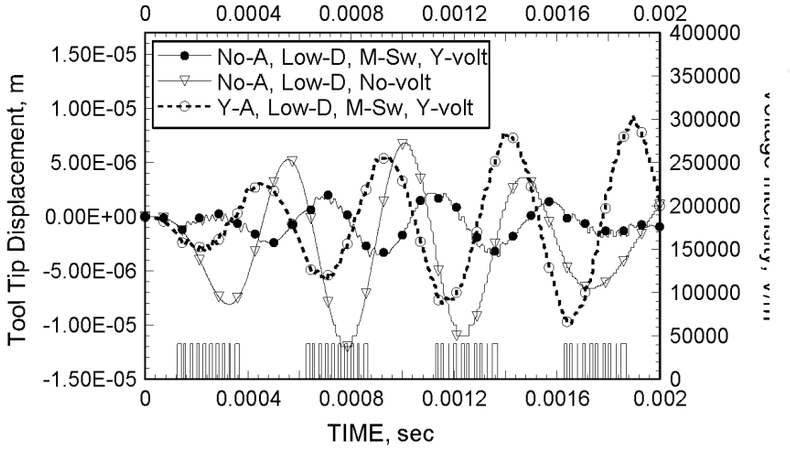

Figure 12. PZT Voltage Intensity and Tool tip displacements Versus time at 2000Hz

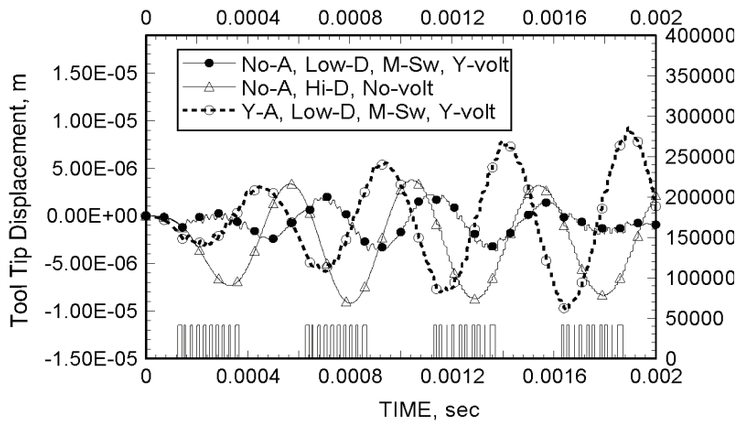

Figure 13. PZT Voltage Intensity and Tool tip displacements Versus time at 2000Hz

6. Conclusions

Attenuating tool vibration error in old turning machines can reduce industrial waste, save money and, improve design flexibility for new cutting tools. Using smart materials in curing machine tool vibration require special attention. The modification of the applied mean voltage during PWM plays a major rule in the effective use of smart materials in tool error elimination. The use of the dynamic absorber showed a slight error reduction in some cases and was not effective in the others. Increasing damping does not show a significant error variation in comparison to the use of smart actuator with modified mean voltage. The FEM solution provided the valid range for the lumped mass modeling to improve both dynamic system modeling and controller design. Tool bit and tool carrier (holder) to actuator stiffness are preferred to be high when both space and weight limitations does not exist. Error elimination requires at least twenty PWM cycles for each disturbing force period to reduce switching transient effects. A reasonable time delay of less than 10% between displacement sensing and actuation has no significance on error elimination. There is a significant difference between the dynamic and the static prediction of the required actuator voltage for error elimination.

7. References

Abboud, N. N., Wojcik, G. L., Vaughan, D. K., Mould, J., Powell, D. J., and Nikodym, L. (1998), Finite Element Modeling for Ultrasonic Transonic Transducers, *Proceedings SPIE Int. Symposium on Medical Imaging 1998*, San Diego, Feb 21-27: 1-24.

Allik, H., and Hughes, T. J. R. (1970), Finite element method for piezoelectric vibration, International Journal for Numerical Methods in Engineering, 2: 151–157.

Bathe, K.J. (1982) ,*Finite Element Procedures in Engineering Analysis*,, Prentice-Hall Inc.: 511-537.

Berlincourt, D. and, Krueger, H. A., (2000), Properties of Morgan ElectroCeramic Ceramics, Technical Publication TP-226, Morgan Electro Ceramics.

Dold, G. (1996), Design of a Microprocessor-Based Adaptive Control System for Active Vibration Compensation Using PMN Actuators, MS Thesis, University of Maryland at College Park.

Eshete, Z. (1996), In Process Machine Tool Vibration Cancellation Using Electrostrictive Actuators, Ph.D. Thesis, University of Maryland at College Park.

Frankpitt, B.A. (1995), A Model of the Dynamics of a Lathe Toolpost that Incorporates Active Vibration Suppression, Institute for System Research, University of Maryland at College Park.

Gopalakrishnan, V., Fedewa, D., Mehrabi, M.G., Kota, S., and Orlandea, N. (2002), Design of Reconfigurable Machine Tools, *ASME J. Manuf. Sci. Eng*., Technical Briefs, 124, Nov.: 483-485.

Hurtado, J. F., and Melkote, S. N, (2001), Improved Algorithm for Tolerance-Based Stiffness Optimization of Machining Fixtures, *ASME J. Manuf. Sci. Eng*., 123, Nov.: 720-730.

Lerch, R., (1990), Simulation of piezoelectric devices by two- and three-dimensional finite elements, *IEEE Transactions on Ultrasonics, Ferroelectrics, and Frequency Control*, 37(3): 233–247.

Luan, J. and Lee, F. C. (1998) ,Design of a High Frequency Switching Amplifier for Smart Material Actuators with Improved Current Mode Control,. *PESC* 98, Vol. 1: 59-64.

Merritt, H. E., (1965), Theory of self-Excited Machine-Tool Chatter, *Journal of Engineering for Industry*, November, pp. 447-454.

Moon, Y. and, Kota, S. (2002), Design of Reconfigurable Machine Tools, *ASME J. Manuf. Sci. Eng*., Technical Briefs, 124, Nov.: 480-483.

Piefort, V. (2001), Finite Element Modeling of Piezoelectric Active Structures, Ph.D. Thesis, ULB, Active Structures Laboratory- Department of Mechanical Engineering and Robotics.

Rashid, M. K. (2004), Smart Actuator Stiffness and Switching Frequency in Vibration Suppression of a Cutting Tool, *Smart Materials and Structures*, Vol.13: 1-9.

Roark, R. J., and Young, W. C. (1975), *Formulas for Stress and Strain (Fifth Edition)*, McGraw-Hill Book Company, New York, Table 24-1j: 337.

Satyanarayana, S., and, Melkote, S. N. (2004), Finite Element Modeling of Fixture–Workpiece Contacts: Single Contact Modeling and Experimental Verification, *International Journal of Machine Tools and Manufacture*. Volume 44, Issue 9, July : 903-913.

Tzou, H. S., and Tseng, C. I. (1990), Distributed piezoelectric sensor/actuator design for dynamic measurement/control of distributed parameter systems: a piezoelectric finite element approach, *Journal of Sound and Vibration*, 138(1):17–34.

Zhang, G., Ko, W., Luu, H., and Wang, X.J. (1995), Design of a smart Tool Post for Precision Machining, *Proceedings of the 27th CIRP International Seminar on Manufacturing Systems*, Ann Arbor, MI, May: 157-164.

Zienkiewicz, O. C., and Taylor, R. L. (2000a), *The Finite Element Method*, Fifth edition Vol.1: The Basis, Butterworth-Heinemann.

Zienkiewicz, O. C., and Taylor, R. L., (2000b), *The Finite Element Method*, Fifth edition Vol.2: Solid Mechanics, Butterworth-Heinemann:.423-424.

Manufacturing the Future

Edited by Vedran Kordic, Aleksandar Lazinica and Munir Merdan

ISBN 3-86611-198-3

Hard cover, 908 pages

Publisher Pro Literatur Verlag, Germany / ARS, Austria

Published online 01, July, 2006

Published in print edition July, 2006

The primary goal of this book is to cover the state-of-the-art development and future directions in modern manufacturing systems. This interdisciplinary and comprehensive volume, consisting of 30 chapters, covers a survey of trends in distributed manufacturing, modern manufacturing equipment, product design process, rapid prototyping, quality assurance, from technological and organisational point of view and aspects of supply chain management.

How to reference

In order to correctly reference this scholarly work, feel free to copy and paste the following:

Maki K. Rashid (2006). Improving Machining Accuracy Using Smart Materials, Manufacturing the Future, Vedran Kordic, Aleksandar Lazinica and Munir Merdan (Ed.), ISBN: 3-86611-198-3, InTech, Available from: http://www.intechopen.com/books/manufacturing_the_future/improving_machining_accuracy_using_smart_materials

INTECH
open science | open minds

InTech Europe
University Campus STeP Ri
Slavka Krautzeka 83/A
51000 Rijeka, Croatia
Phone: +385 (51) 770 447
Fax: +385 (51) 686 166
www.intechopen.com

InTech China
Unit 405, Office Block, Hotel Equatorial Shanghai
No.65, Yan An Road (West), Shanghai, 200040, China
中国上海市延安西路65号上海国际贵都大饭店办公楼405单元
Phone: +86-21-62489820
Fax: +86-21-62489821

IntechOpen